Solar-Terrestrial Physics. 2024. Vol. 10. Iss. 2. P. 3–12. DOI: 10.12737/stp-102202401. © 2024
S.A. Belov, L.S. Ledentsov, D.I. Zavershinskii, S.A. Bogachev. Published by INFRA-M Academic Publishing House

UDC 523.947, 523.9-739
DOI: 10.12737/stp-102202401

Received December 04, 2023
Accepted March 21, 2024

DIFFERENTIAL EMISSION MEASURE OF SOLAR NANOFLARES MEASURED WITH THE SITES ALGORITHM

S.A. Belov
Samara National Research University,
Samara, Russia, mr_beloff@mail.ru
Samara Branch of Lebedev Physical Institute RAS,
Samara, Russia

L.S. Ledentsov
Samara National Research University,
Samara, Russia, leonid.ledentsov@gmail.com
Sternberg Astronomical Institute,
Moscow, Russia

D.I. Zavershinskii
Samara National Research University,
Samara, Russia, dimanzav@mail.ru
Samara Branch of Lebedev Physical Institute RAS,
Samara, Russia

S.A. Bogachev
Samara National Research University,
Samara, Russia, bogachev.sergey@gmail.com
Space Research Institute,
Moscow, Russia

Abstract. The paper presents the results of a study of capabilities of the SITES algorithm for reconstructing the differential emission measure (DEM) of a source from its radiation in several parts of the electromagnetic spectrum in the context of observing solar nanoflares with the AIA/SDO instrument. The SITES method was implemented in the Python programming language and was first used to construct the DEM of nanoflares. For this purpose, we tested the efficiency of the algorithm on model single- and double-peak DEM at characteristic temperatures of solar nanoflares. The test results indicate that the SITES algorithm can be of limited applicability for studying the DEM of nanoflares in the single-peak approximation. The algorithm has a combination of high accuracy and high counting rate in the studied temperature range from 1 to 3 MK. The features of DEM nanoflares reconstructed by the SITES method were examined using our previously found sample of 58855 events observed in 2019 with the AIA/SDO instrument. The results confirm that the characteristic plasma temperature in nanoflares is 1–2 MK. The reconstructed DEM of nanoflares generally have one maximum within this range, but the temperature distribution we obtained for all flares forms two clusters with maxima at 1.2 and 1.7 MK. We interpret this as possible evidence for the existence of two types of solar nanoflares, but this result requires further confirmation.

Keywords: nanoflares, differential emission measure (DEM), quiet Sun.

INTRODUCTION

Heating of the solar corona to observable temperatures $T>1$ MK has remained an unsolved mystery of solar physics for many decades. There are currently several approaches designed to explain the heating mechanism, among which two main mechanisms stand out: magnetohydrodynamic wave heating and nanoflare heating. The first implies the ability of waves to transfer energy from the lower layers of the solar atmosphere to the corona, where it can heat the surrounding plasma (see, e.g., [Van Doorsselaere et al., 2020]). The second approach attributes the solar corona heating to the large number of small-scale flare events with energies ~10^{23}–10^{27} erg, which Parker called nanoflares [Parker, 1988].

Heating the solar corona and maintaining its temperature constant due to the energy of nanoflares require that their energy release rate is of the order of $6\cdot10^{27}$ erg/s [Bogachev et al., 2020]. Thus, the question arises whether the occurrence rate of nanoflares is sufficient or not. Hudson [1991] has shown that the energy distribution of the occurrence rate of flare events from 10^{27} to 10^{33} erg is well described by the power-law dependence $N(E)=AE^{-\alpha}$, where A is a normalization coefficient; $\alpha\approx1.8$ is the spectral slope. This dependence can be extended to the region of lower energies. For such a power-law distribution, it is easy to show that at $\alpha>2$ the integral energy of flares increases as they move toward low energies. Thus, detailed knowledge of the distribution index α can shed light on the contribution of nanoflare events to the overall energy budget of the solar corona. At present, different authors estimate the α parameter at 1.3–2.8 (see Table 1). This spread is most likely due to the difference between methods of determining both nanoflares themselves and their energy.

In recent works dealing with nanoflares [Joulin et al., 2016; Purkhart, Veronig, 2022], the temperature of events and hence their thermal energy are determined by reconstructing the differential emission measure (DEM) of plasma $\xi(T)$ from observational data:

$$\xi(T)=\frac{dM}{dT},$$

$$M=\int_0^\infty n_e^2(x)\,dx,$$

where M is the total emission measure of plasma column along the line of sight x; n_e is the electron density. The temperature of the observed plasma volume T_{est} can be

Table 1

Values in ascending order of the power of energy distribution of nanoflares α obtained by different authors

Parameter α	Observable wavelengths, Å	Source
1.35±0.20	195	Berghmans et al., 1998
1.65±0.20	131, 171, 193, 211, 335	Joulin et al., 2016
1.79±0.08	171, 195	Aschwanden et al., 2000
1.81±0.10	195	Aschwanden, Parnel, 2002
1.86±0.07	171	Aschwanden, Parnel, 2002
1.9±0.1	304	Berghmans et al., 1998
2.28±0.03	94, 131, 171, 193, 211, 335	Purkhart, Veronig, 2022
2.3±0.1	171, 195	Benz, Krucker, 2002
2.54	171, 195	Krucker, Benz, 1998
2.81±0.52	171	Ulyanov, 2019

estimated from the resulting DEM [Cheng et al., 2012; Vanninathan et al., 2015]:

$$T_{\text{est}} = \frac{\int_0^\infty T\xi(T)\,dt}{\int_0^\infty \xi(T)\,dt}.$$

Note that the intensity I recorded in a certain telescope spectral channel is related to DEM as follows:

$$I = \int_0^\infty R(T)\xi(T)\,dT,$$

where $R(T)$ is the temperature response function of the telescope's spectral channel under study. This relationship is used to reconstruct DEM from a set of observed intensities of the telescope's spectral channels. Nowadays, there is a wide range of different methods and algorithms that allow us to calculate DEM of observable plasma (see, e.g., [Massa et al., 2023], where different algorithms are compared).

This implies that DEM is an important characteristic of observable plasma, which is used to determine temperature distribution, average temperature and its associated thermal energy for the volume of interest. Nonetheless, despite this fact, no special attention is given to calculating DEM of nanoflares in recent research. The calculation of DEM itself is often intermediate and is used for further calculation of thermodynamic plasma parameters. Only a few papers describe DEMs of single events [Chitta et al., 2021]. At the same time, for coronal holes, as an example, there are statistical studies of DEM [Heinemann et al., 2021], whose purpose is to find a typical DEM from a large set of observed regions. In our opinion, these statistical studies have a greater advantage over the study of characteristics of single events, especially given that nanoflares occur much more often than ordinary flares. On the other hand, the small size of nanoflares compared to ordinary flares makes it difficult to specify DEM and its nature since nanoflares are not visible in all channels, which leads either to addition of noise or to loss of information at the input of DEM estimation algorithms. The high occurrence rate of nanoflares sets a limitation to the algorithm we employ since the methods of estimating DEM require a large amount of calculations. It can take a long time to explore a large ensemble of nanoflares.

The paper deals with the application of the SITES method to estimate DEM of nanoflares, statistically studies DEM of nanoflares in order to determine peculiarities of this distribution and to get an idea about typical DEM of a single nanoflare.

The paper is structured as follows: Section 1 explores state-of-the-art capabilities of the SITES method for detecting nanoflares; Section 2 applies the SITES method to the previously found array of nanoflares and calculates their DEMs; Section 3 presents the results of the study and conclusions.

1. THE SITES METHOD

The SITES method under study [Morgan, Pickering, 2019], unlike the popular regularization method [Hannah, Kontar, 2012], does not reconstruct DEM by solving the problem of minimizing the regularized error functional, but construct it iteratively, using the initial approximation explicitly given by response functions of the telescope in different channels. At the same time, the relative contribution of each channel in comparison with the contributions of the other channels is taken into account in the construction process for each temperature range considered. The SITES method has attracted our attention for several reasons. First of all, the authors of the method claim its high counting rate, which is a critical parameter in studying a large ensemble of nanoflares. In addition, this method has a clear concept and is quite simple to implement. We have implemented SITES in the Python programming language and have for the first time used it to construct DEM of nanoflares.

Our study relies on extreme ultraviolet emission intensity data obtained by the Atmospheric Imaging Assembly (AIA) aboard the Solar Dynamics Observatory (SDO) [Lemen et al., 2012]. AIA is a four-telescope array that operates in EUV, UV, and visible bands and provides full-disk solar images of 4096×4096 pixels with spatial and temporal resolutions of 0.6" and 12 s respectively.

When processing the AIA data for the analysis of nanoflares, we limited ourselves to the following set of EUV channels: 131, 171, 193, and 211 Å. This choice was dictated by the fact that this combination makes it possible to detect the largest number of nanoflares without involving additional spectral ranges [Belov et al., 2023].

Moreover, we believe that the 304 Å channel contains information about colder and deeper layers of the solar atmosphere, and the 94 and 335 Å channels have a high noise level, which can adversely affect the accuracy in calculating DEM in these channels.

We assume that due to the lower energy of nanoflares as compared to ordinary flares DEM of nanoflares has a simpler temperature dependence. Specifically, this difference may lie in the fact that there are no low- and high-temperature humps in DEM of nanoflares, which is due to the absence of a chromospheric response to a weak event and the relatively low energy of accelerated electrons respectively. For this reason, to assess the quality of the algorithm, we have utilized single- and double-temperature approximations, whose parameters are listed in Tables 2 and 3 respectively together with the parameters of the algorithm, as test models of true DEM of nanoflares.

Figure 1 compares the average temperature obtained from the reconstructed DEM by SITES (see the parameters listed in Table 2) with the average temperature determined by the model single-temperature DEM. As can be seen from the heat map in the top panel of Figure 1, the method allows us to determine (with an accuracy <10 %) the average temperature for single-peak Gaussian DEM with T_{MAX} in the vicinity of 1 MK and σ from 0.1 to 0.5 MK, as well as for T_{MAX} in the vicinity of 3.25 MK and σ in the entire range considered.

Figure 2 shows the relative errors in determining temperature maximum of DEM. In this case, the position of DEM maximum is determined quite accurately on the T_{MAX} interval from 1 to 3 MK for almost the entire range of widths of test DEM under study. This conclusion is also confirmed by bottom panels, which exhibit the dependence of estimated DEM maximum on the position of test DEM maximum.

Nevertheless, the DEM profile of real nanoflares may have a more complex shape than the Gaussian function. To assess how well the algorithm can reconstruct a more complex distribution pattern, we have conducted a series of tests for double-temperature DEM, which is the sum of two Gaussian functions. The algorithm's parameters remained the same. Table 3 presents parameters of test DEM.

Figures 3 and 4 illustrate the Pearson correlation between the test and reconstructed DEM profiles and the *sMAPE* metric employed to estimate the correspondence between two curves and that calculated by the formula

$$sMAPE = \frac{1}{N}\sum_{i=0}^{N}\frac{\left|DEM_i - DEM_i\right|}{DEM_i + DEM_i}100\ \%,$$

where DEM is reconstructed DEM; *DEM* is test DEM.

Table 2

Parameters of the algorithm and the test problem for a single Gaussian curve

Algorithm parameters		Test parameters	
Minimum temperature	0.2 MK	Form of test DEM	$A\exp\left(-\left(\frac{T-T_{MAX}}{\sigma}\right)^2\right)$
Maximum temperature	5 MK	Amplitude A	$1.4\cdot10^{21}$ cm^{-5}K^{-1}
Number of bins	31	Position of T_{MAX}	0.5–4.0 MK
Accuracy	5 %	Variation step of T_{MAX}	0.01 MK
Maximum number of iterations	300	Profile width of σ	0.1–1.0 MK
Channels in use	131, 171, 193, 211 Å	variation step of σ	0.01 MK

Table 3

Parameters of the test problem for a double Gaussian curve

Form of test DEM	$A\left[\exp\left(-\left(\frac{T-T_{cold}}{\sigma}\right)^2\right)+\exp\left(-\left(\frac{T-T_{hot}}{\sigma}\right)^2\right)\right]$
Amplitude A	$1.4\cdot10^{21}$ cm^{-5}K^{-1}
Position of cold maximum T_{cold}	0.5–2.0 MK
Variation step of T_{cold}	0.01 MK
Position of hot maximum T_{hot}	(0.5+σ)–4.0 MK
Variation step of T_{hot}	0.01 MK
Profile width σ	0.25, 0.5, 0.75, 1.0 MK

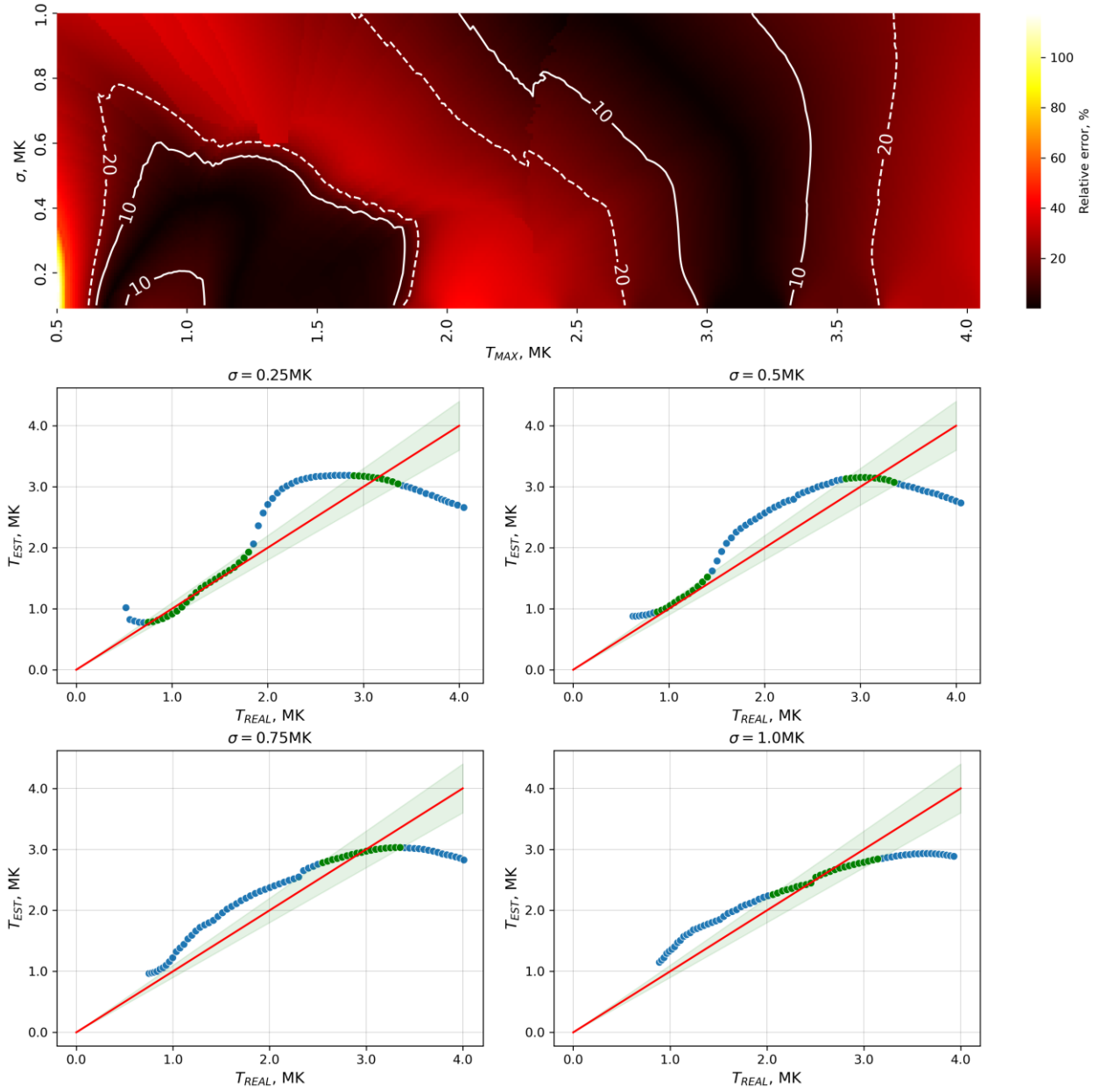

Figure 1. Estimated average plasma temperature for test Gaussian DEM. Top panel: relative error in determining the average temperature for different parameters of test DEM. Dark areas correspond to small errors; red and yellow colors, to areas with large errors. Bottom panels: the estimated average temperature as function of the average temperature of test DEM; the green color marks an area with an error less than 10 %

It can be seen that, despite the high correlation between the reconstructed and test profiles in a wide range of positions of T_{cold} and T_{hot} peaks, the error during the reconstruction, estimated by *sMAPE*, is large enough to indicate a satisfactory reconstruction of the DEM profile with these parameters of the algorithm and the test problem. Figure 5 compares the test and reconstructed DEM temperature profiles for some selected parameters. We can conclude that the algorithm is able to recognize a high-temperature peak provided that it is located at ~2.5 MK, which coincides with the region where the 211 Å channel makes the greatest contribution to the estimate of DEM. At high temperatures, channel responses weaken, thereby impeding the detection of hotter peaks. If a hot peak is <2.0 MK, then apparently, due to the overwhelming influence of the 171 Å channel, the second peak cannot be identified. Thus, for the set of channels considered and the selected temperature range, it is impossible to reliably detect a double-peak DEM structure for real nanoflares, if any. Note that the algorithm itself is able to reconstruct with sufficient accuracy the double-peak DEM structure with hotter peaks than those treated here [Morgan, Pickering, 2019]. Based on the results of this part of the study, we can draw a preliminary theoretical conclusion that the SITES method can be used to reconstruct DEM of weak flares, including nanoflares. In the next section, we test this assumption on specific events.

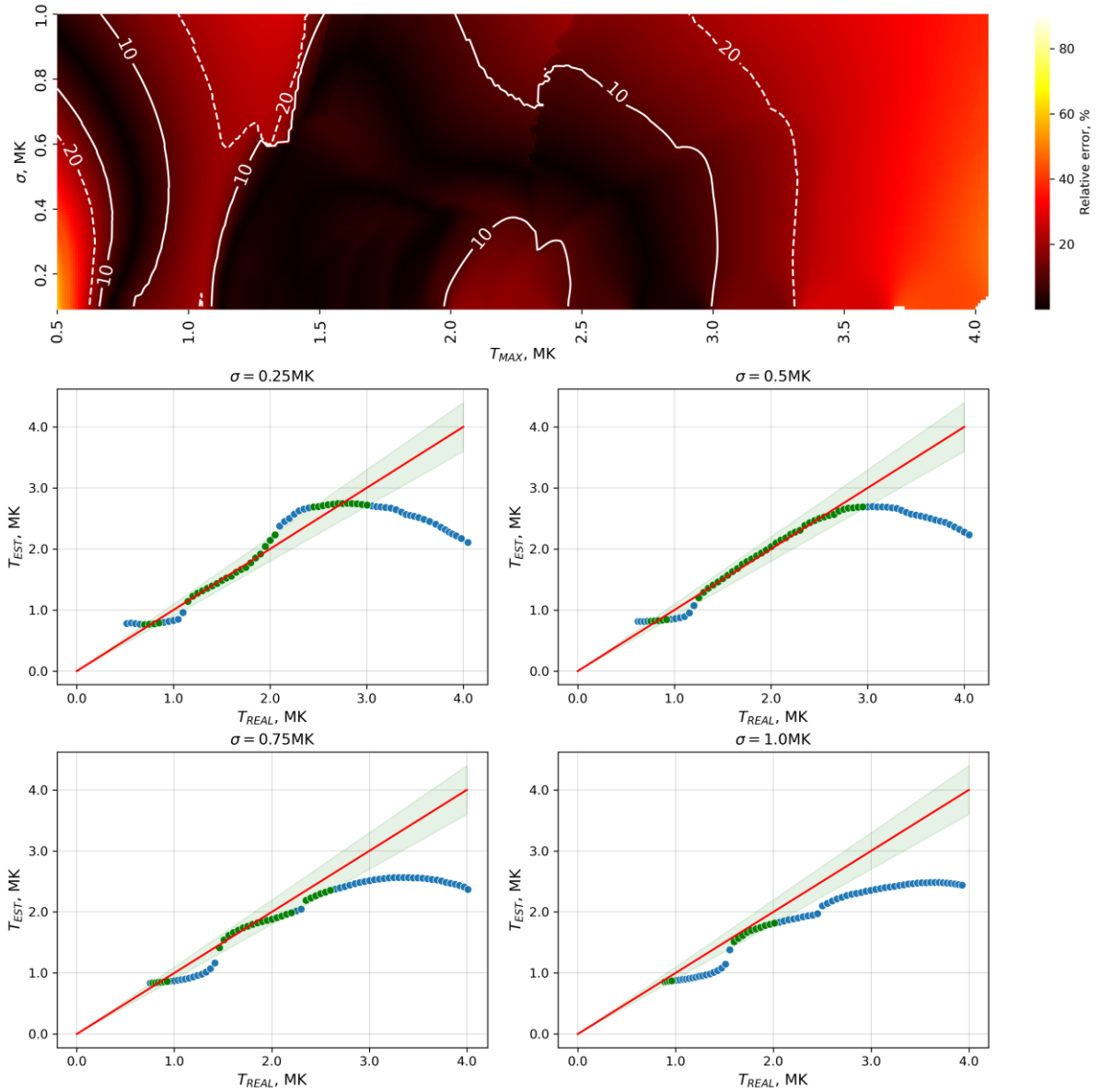

Figure 2. Estimated position of DEM maximum for test Gaussian DEM. Designations are the same as in Figure 1

2. APPLICATION OF THE SITES METHOD

The test allows us to conclude that the use of SITES to estimate DEM of nanoflares in the 131, 171, 193, and 211 Å channels is a single-peak approximation to real DEM of nanoflares. To estimate this distribution, we have used 58 855 events we have found in [Belov et al., 2023] independently in each of the channels considered for the time interval 12:00–13:00 UT on May 20, 2019 in two rectangular regions of 600×1200 pixels located in the northern and southern hemispheres of the Sun. For each of the identified events, we employed SITES to calculate DEMs at the peak and at the beginning of the events, and then dropped the nanoflares the accuracy of determining DEMs of which was >5 %; this led to loss of ~16 % of data.

For the peaks of the nanoflares under study, we used the estimated DEM to calculate average temperatures of the events and to plot their temperature distribution (Figure 6). This distribution is well approximated by the sum of two Gaussian curves with the parameters listed in Table 4.

Based on the obtained distribution by peak temperature, nanoflares can be divided into clusters of cold and hot nanoflares with a boundary of 1.48 MK (corresponds to the minimum between the humps). Figure 7 displays the number of cold and hot flares visible in each of the channels of interest. From the diagram, it is easy to see that the 211 Å channel dominates for hot flares, whereas the 171 Å channel plays a dominant role for cold ones.

For DEMs of cold and hot nanoflares we have calculated the 10, 20, 50, 80, and 90 % levels, as well as average values (Figure 8). As expected, the obtained DEMs have a single-peak structure; DEM for hot flares has a gentler profile elongated to ~3 MK. At the same time, the DEM profile for cold flares abruptly ends at ~2.5 MK. When comparing average DEM values, it is clearly seen that DEM of hot nanoflares significantly exceeds that of cold ones in the range from 2 to 4 MK.

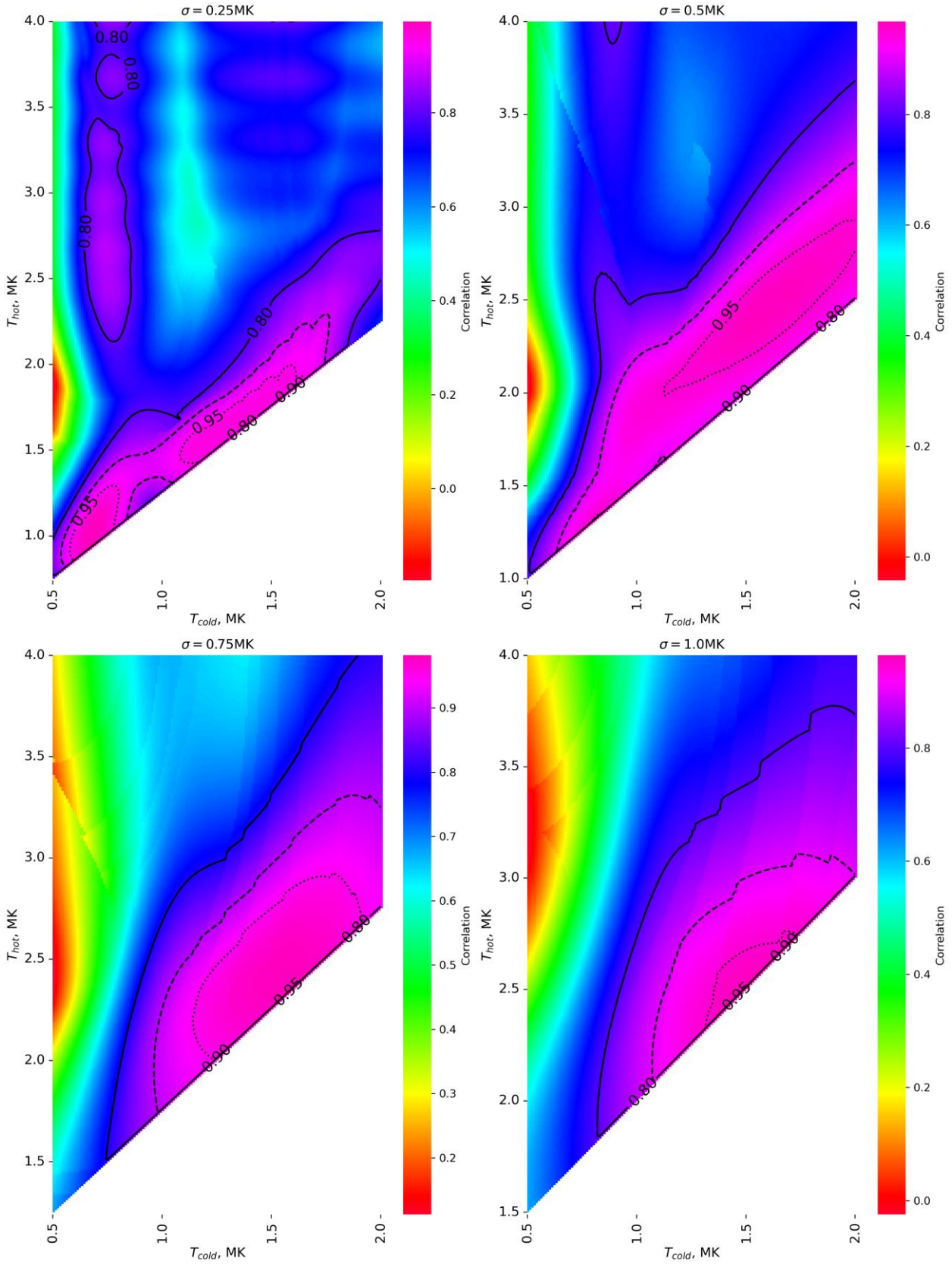

Figure 3. Correlation between the test double Gaussian DEM and the estimated DEM for different parameters of the test DEM

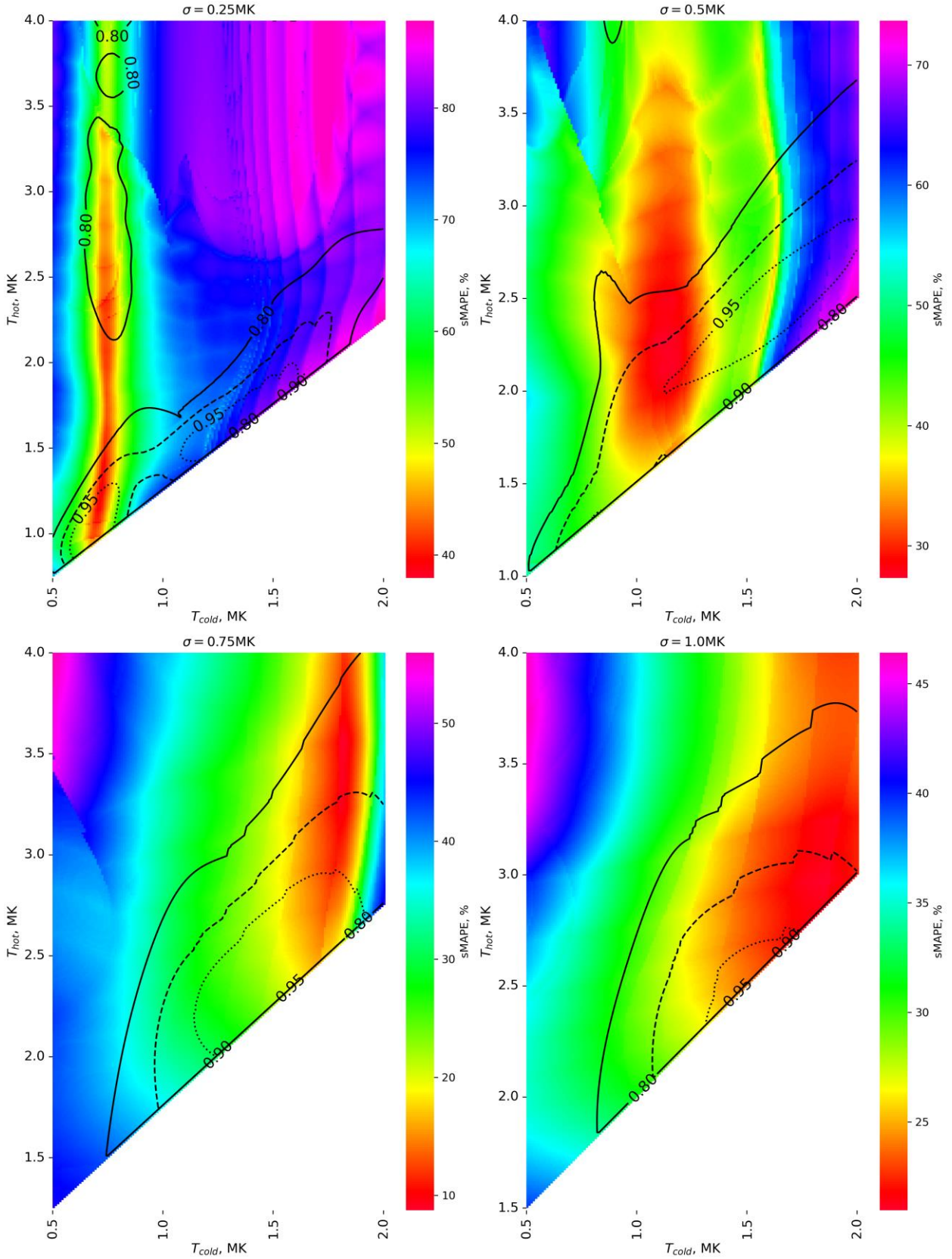

Figure 4. The *sMAPE* metric between the test double Gaussian DEM and the estimated DEM for different parameters of the test DEM. Contour lines indicate the correlation coefficient

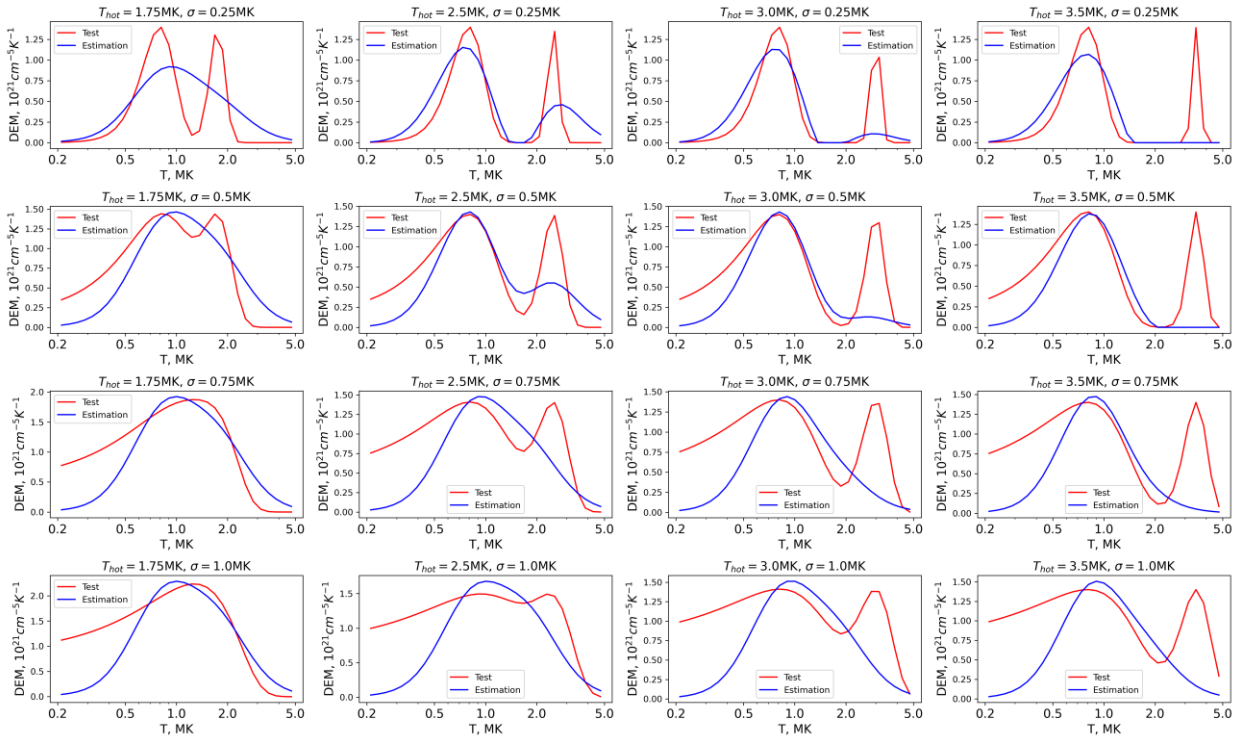

Figure 5. Profiles of estimated DEM for test double Gaussian DEM. The red line is the test curve; the blue line, the curve reconstructed by the SITES method

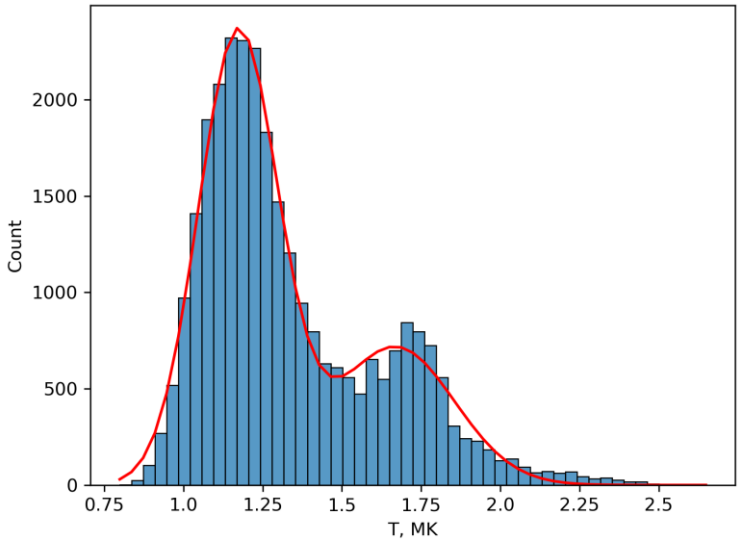

Figure 6. Distribution of nanoflares by peak temperature and its approximation by a double Gaussian curve

Table 4

Curve parameters for approximating the distribution of nanoflares by peak temperature

Approximating curve	$A_1 \exp\left(-\frac{1}{2}\left(\frac{T-T_1}{\sigma_1}\right)^2\right) + A_2 \exp\left(-\frac{1}{2}\left(\frac{T-T_2}{\sigma_2}\right)^2\right)$
Amplitude A_1	2353.014
Amplitude A_2	718.014
Maximum T_1	1.173 MK
Maximum T_2	1.668 MK
Half-width σ_1	0.126 MK
Half-width σ_2	0.187 MK

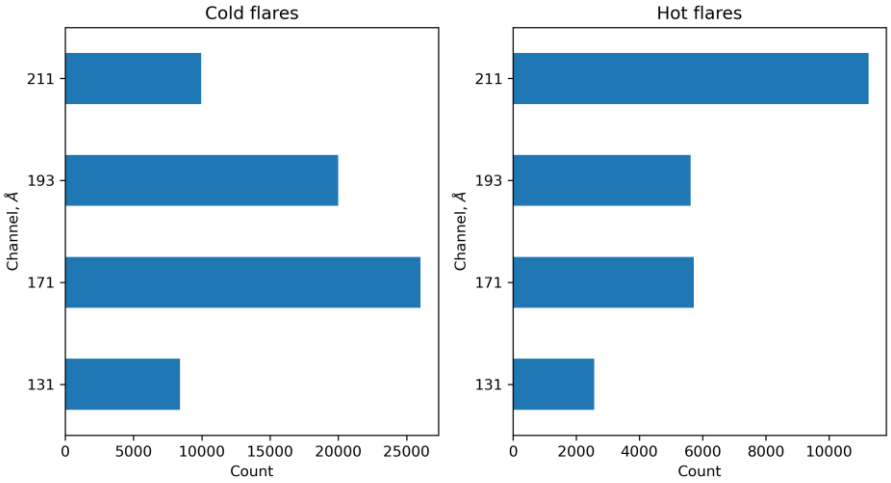

Figure 7. Distribution of cold and hot nanoflares in the channels under study

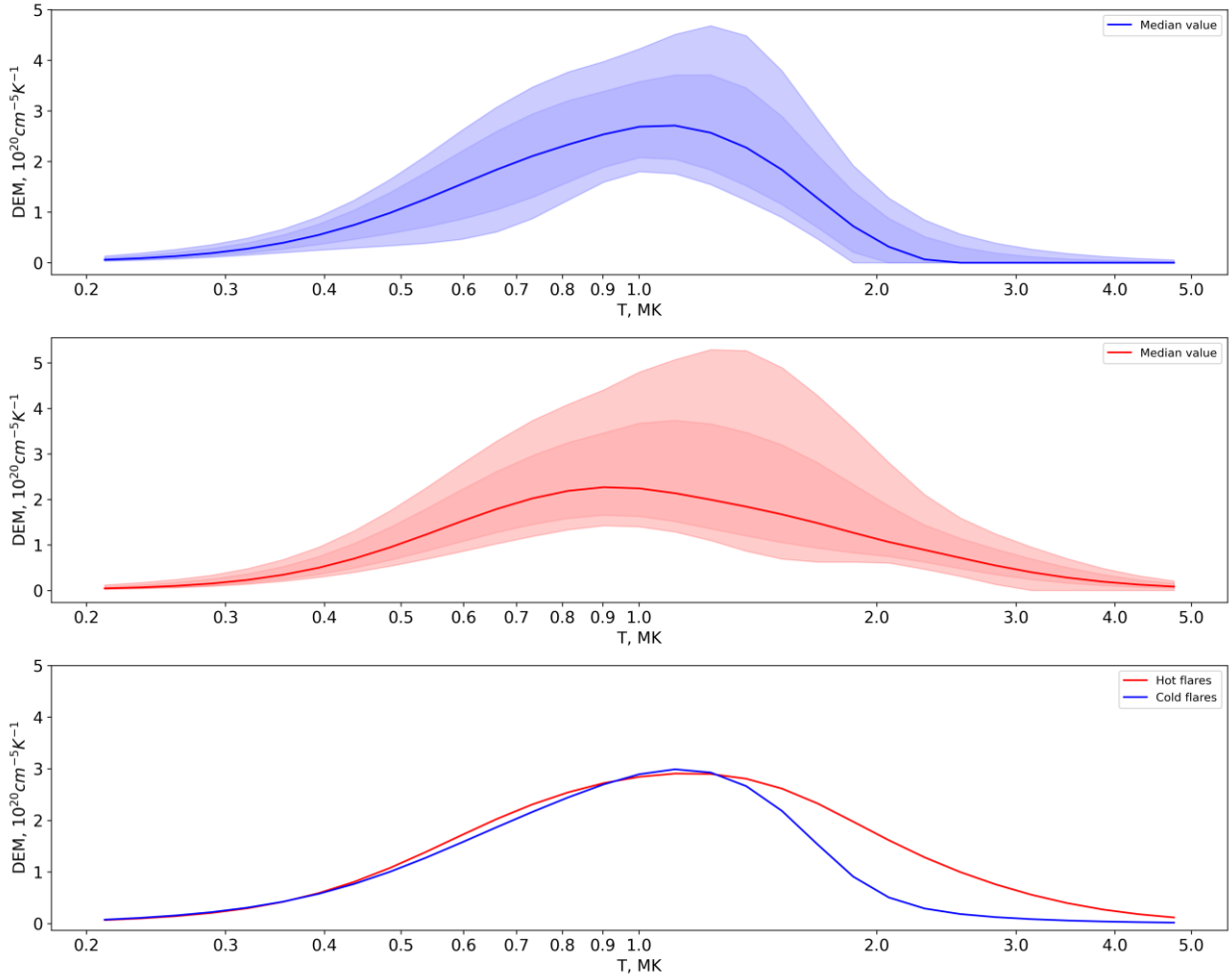

Figure 8. DEMs calculated for the entire set of nanoflares. Top panel: median DEM (blue curve), levels of 10 and 90 % (light area), 20 and 80 % (dark area) for cold flares. Middle panel: median DEM (red curve), levels of 10 and 90 % (light area), 20 and 80 % (dark area) for hot flares. Bottom panel: average DEM values for cold (blue curve) and hot (red curve) flares

3. RESULTS AND CONCLUSIONS

We have examined the application of the SITES algorithm for determining DEM of nanoflares, using data from the 131, 171, 193, and 211 Å channels in the temperature range 0.2–5.0 MK. We have found out that the algorithm works mainly in single-peak mode and reconstruct the average temperature and positions of the Gaussian DEM maximum quite well. The algorithm can reconstruct the double-peak DEM structure if the hot peak is located in the vicinity of 2.5 MK. Hence, from the results of SITES operation it is difficult to estimate the real form of DEM of nanoflares, at least when using it in this mode.

With SITES we have estimated DEM at the peak of the nanoflares visible in the 131, 171, 193, and 211 Å channels. The distribution of the identified nanoflares by peak temperature has been found to have the shape of a double Gaussian curve and allows us to divide the ensemble studied into cold and hot nanoflares with a boundary of 1.48 MK. For the temperature clusters, we have calculated levels of 10, 20, 50, 80, and 90%, as well as average DEM values. As expected, the smoothed DEM profiles have a single-peak structure, with DEM of hot flares exceeding that of cold flares in the range from 2 to 4 MK.

As far as we know, the characteristic DEM profile of nanoflares has not been described in the literature before (see references in Table 1). For this reason, we cannot make a direct comparison of our results with the results of other authors; however, the identified peak temperatures of average DEMs for cold and hot nanoflares (bottom panel in Figure 8) lie in the range 1–2 MK, which is consistent with the qualitative conclusions made by other authors and the temperature sensitivity areas of the AIA ultraviolet channels in use.

Further calculations of the total thermal energy of nanoflares and the spectrum slope are beyond the scope of this work. It requires us to introduce a number of assumptions that are ambiguously interpreted in the literature. Among them is the question about the coefficient of filling of the volume observed in each pixel with hot plasma, as well as the question concerning the method of clustering multi-pixel brightenings into one nanoflare event. Both these questions significantly affect the determination of the nanoflare energy and require an individual in-depth study.

The work was financially supported by the Russian Science Foundation (Grant 22-22-00879). The SITES method for calculating DEM was implemented during the work under Project FSSS-2023-0009, supported by the Ministry of Science and Higher Education of the Russian Federation as part of Government assignment to universities and scientific organizations.

REFERENCES

Aschwanden M.J., Parnell C.E. Nanoflare statistics from first principles: fractal geometry and temperature synthesis. *Astrophys. J*. 2002, vol. 572, no. 2, p. 1048. DOI: 10.1086/340385.

Aschwanden M.J., Tarbell T.D., Nightingale R.W., Wolfson C.J. Time variability of the “quiet” Sun observed with TRACE. II. Physical parameters, temperature evolution, and energetics of extreme-ultraviolet nanoflares. *Astrophys. J*. 2000, vol. 535, no. 2, p. 1047. DOI: 10.1086/308867.

Belov S.A., Bogachev S.A., Ledentsov L.S., Zavershinskii D.I. Solar nanoflares in different spectral ranges. *Astron. Astrophys*. 2023. Vol. 684. P. A60. DOI: 10.1051/0004-6361/202348199.

Benz A.O., Krucker S. Energy distribution of microevents in the quiet solar corona. *Astrophys. J*. 2002, vol. 568, no. 1, p. 413. DOI: 10.1086/338807.

Berghmans D., Clette F., Moses D. Quiet Sun EUV transient brightenings and turbulence. A panoramic view by EIT on board SOHO. *Astron. Astrophys*. 1998, vol. 336, pp. 1039–1055.

Bogachev S.A., Ulyanov A.S., Kirichenko A.S., Loboda I.P., Reva A.A. Microflares and nanoflares in the solar corona. *Physics-Uspekhi*. 2020, vol. 63, iss. 8, p. 783.

Cheng Zhang J., Saar S.H., Ding M.D. Differential emission measure analysis of multiple structural components of coronal mass ejections in the inner corona. *Astrophys. J*. 2012, vol. 761, no. 1, p. 62. DOI: 10.1088/0004-637X/761/1/62.

Chitta L.P., Peter H., Young P.R. Extreme-ultraviolet bursts and nanoflares in the quiet-Sun transition region and corona. *Astron. Astrophys*. 2021, vol. 647, p. A159. DOI: 10.1051/0004-6361/202039969.

Hannah I.G., Kontar E.P. Differential emission measures from the regularized inversion of Hinode and SDO data. *Astron. Astrophys*. 2012, vol. 539, p. A146. DOI: 10.1051/0004-6361/201117576.

Heinemann S.G., Heinemann S.G., Saqri, J., Veronig A.M., Hofmeister S.J., Temmer M. Statistical approach on differential emission measure of coronal holes using the CATCH catalog. *Solar Phys*. 2021, vol. 296, no. 18, pp. 1–17. DOI: 10.1007/s11207-020-01759-0.

Hudson H.S. Solar flares, microflares, nanoflares, and coronal heating. *Solar Phys*. 1991, vol. 133, pp. 357–369. DOI: 10.1007/BF00149894.

Joulin V., Buchlin E., Solomon J., Guennou C. Energetic characterisation and statistics of solar coronal brightenings // *Astron. Astrophys*. 2016, vol.. 591, pp. A148. DOI: 10.1051/0004-6361/201526254.

Krucker S., Benz A.O. Energy distribution of heating processes in the quiet solar corona. *Astrophys. J*. 1998, vol. 501, no. 2, p. L213. DOI: 10.1086/311474.

Lemen J.R., Title A.M., Akin D.J., Boerner P.F., Chou C., Drake J.F., et al. The Atmospheric Imaging Assembly (AIA) on the Solar Dynamics Observatory (SDO). *Solar Phys*. 2012, vol. 275, pp. 17–40. DOI: 10.1007/ s11207-011-9776-8.

Massa P., Gordon Emslie A., Hannah I.G., Kontar E.P. Robust construction of differential emission measure profiles using a regularized maximum likelihood method. *Astron. Astrophys*. 2023, vol. 672. DOI: 10.1051/0004-6361/202345883.

Morgan H., Pickering J. Sites: Solar iterative temperature emission solver for differential emission measure inversion of EUV observations. *Solar Phys*. 2019, vol. 294, no. 135, p. 135. DOI: 10.1007/s11207-019-1525-4.

Parker E.N. Nanoflares and the solar X-ray corona. *Astrophys. J*. 1988, vol. 330, pp. 474–479. DOI: 10.1086/166485.

Purkhart S., Veronig A.M. Nanoflare distributions over solar cycle 24 based on SDO/AIA differential emission measure observations. *Astron. Astrophys*. 2022, vol. 661, p. A149. DOI: 10.1051/0004-6361/202243234.

Ulyanov A.S., Bogachev S.A., Reva A.A., Kirichenko A.S., Loboda I.P. The energy distribution of nanoflares at the minimum and rising phase of solar cycle 24. *Astron. Lett.* 2019. Vol. 45, no. 4. P. 248–257. DOI: 10.1134/S1063773719040078.

Van Doorsselaere T., Srivastava A.K., Antolin P., Magyar N., Farahani S.V., Hui Tian, et al. Coronal heating by MHD waves. *Space Sci. Rev*. 2020, vol. 216, no. 140, pp. 1–40. DOI: 10.1007/s11214-020-00770-y.

Vanninathan K., Veronig A.M., Dissauer K., Madjarska M.S., Hannah I.G., Kontar E.P. Coronal response to an EUV wave from DEM analysis. *Astrophys. J*. 2015, vol. 812, no. 2, p. 173. DOI: 10.1088/0004-637X/812/2/173.

Original Russian version: Belov S.A., Ledentsov L.S., Zavershinskii D.I., Bogachev S.A., published in Solnechno-zemnaya fizika. 2024. Vol. 10. Iss. 2. P. 4–14. DOI: 10.12737/szf-102202401.

How to cite this article

Belov S.A., Ledentsov L.S., Zavershinskii D.I., Bogachev S.A. Differential emission measure of solar nanoflares measured with the SITES algorithm. *Solar-Terrestrial Physics*. 2024. Vol. 10. Iss. 2. P. 3–12. DOI: 10.12737/stp-102202401.